Materials Advances

ROYAL SOCIETY OF CHEMISTRY

PAPER

View Article Online
View Journal | View Issue



Cite this: *Mater. Adv.*, 2022, 3, 2495

# A fluorescent colorimetric vanillin di-Schiff base chemosensor for detection of Cu(II) and isolation of trinuclear Cu(II)–dihydrazide†

Meman Sahu, Amit Kumar Manna and Goutam Kumar Patra *

Received 22nd December 2021,
Accepted 26th January 2022

DOI: 10.1039/d1ma01227d

rsc.li/materials-advances

In this work, we developed a simple fluorescent colorimetric chemosensor **$H_2L$** [6,6′-((1,1′)-hydrazine-1,2-diylidene bis(methanylylidene)) bis(2-(6-methoxy)) phenol] for rapid detection of $Cu^{2+}$ in aqueous solution. The method for synthesis of **$H_2L$** is very simple and environment friendly. This organic Schiff base probe was characterized by $^1$H-NMR, FT-IR and ESI-MS spectroscopy along with single-crystal XRD analysis. It exhibited binding-induced colour change with $Cu^{2+}$ion from colourless to intense yellow and fluorescence enhancement. The LOD values of **$H_2L$** towards $Cu^{2+}$ were calculated to be $7.1 \times 10^{-8}$ M (colorimetrically) and $3.8 \times 10^{-8}$ M (fluorometrically). The interactions between **$H_2L$** and $Cu^{2+}$ were studied by Job's plot, ESI-MS, FT-IR spectroscopy and DFT calculations. The crystal structure of the **L**–$Cu^{2+}$ adduct was also determined by single-crystal X-ray analysis, and it was found that two molecules of **L** coordinate with three molecules of $Cu^{2+}$ ions. The receptor **$H_2L$** could operate in a wide pH range and can be successfully applied for detection and quantification of $Cu^{2+}$ ions in environmental samples and logic applications.

## Introduction

Copper(II) is one of the essential metal ions in the human body, and it plays an important role in various biological and environmental processes.[1–5] The first-row transition element Cu is the third most important tracer element in biological processes, and Cu concentrations up to 1.3 mg $L^{-1}$ in drinking water are tolerable, according to the U.S. Environmental Protection Agency (EPA).[6–8] Cu(II) is present in hemocyanin, which functions as oxygen transporter in insects. In the human body, Cu(II) is present in several enzymes, including superoxide dismutase, tyrosinase, and dopamine hydroxylase. In cytochrome *c* oxidase and ferritin, Cu(II) presents in combination with another metal, iron ($Fe^{2+}$). Although excess copper can result in mitochondrial damage, DNA breakage, neuronal injury, and Alzheimer's and Wilson's diseases, deficiency of Cu(II) causes serious illness such as anemia, as it is an important part of ceruloplasmin.[9–13] Major concentrations of Cu(II) are found in the liver, kidney, heart and brain. Cu(II) is a key component in the body needed for regulation of many biological functions. However, its presence in excess affects some biologically important enzymes by binding with their active sites and displacing other nutrient minerals.[14–17] Cu(II) can disturb nutrient absorption and transport, thus destroying plant and aquatic ecosystems.[18–20]

Conventional methods such as atomic absorption spectrometry (AAS),[21,22] inductively coupled plasma–mass spectrometry (ICP-MS),[23] flame atomic absorption spectrometry (FAAS)[24,25] and electrochemical assays[26,27] are generally used for the detection of metal ions like $Cu^{2+}$. Although these traditional methods are responsive, accurate and selective, they require special sampling techniques, manual operation, and professional handling, and they are time consuming, expensive and sometime inconclusive. To overcome these problems, researchers are searching for easily employable optical sensors.

Optical sensors have several advantages such as sensitivity, selectivity, cost effectiveness and simplicity.[28,29] Colorimetric and fluorometric optical chemosensors offer real-time analyte recognition, easy operation, controllability and lower response time.[30–34] A variety of colorimetric and fluorometric sensors for Cu(II)[35–44] have been reported. Despite these, considering the effectiveness and low detection limit, the design and synthesis of more effective chemosensors are still desirable.

In our ongoing research, we have already reported several chemosensors for Cu(II) based on amides,[45] triazole,[46] dihydrazone,[47] dihydrophenylquinazolinone,[48] thiosemicarbazone,[49] and benzohydrazide.[50,51] Taking another step in the process of searching for suitable chemosensors, we focused on

*Department of Chemistry, Guru Ghasidas Vishwavidyalaya, Bilaspur (C.G.), India. E-mail: patra29in@yahoo.co.in; Tel: +91 7587312992*

† Electronic supplementary information (ESI) available: Fig. S1–S10. CCDC 2087278 and 2087279. For ESI and crystallographic data in CIF or other electronic format see DOI: 10.1039/d1ma01227d

dihydrazone-based chemosensors. Herein, we have successfully designed and synthesized 6,6′-((1,1′)-hydrazine-1,2-diylidene bis(methanylylidene)) bis(2-(6-methoxy)) phenol (**$H_2L$**), a dihydrazone of *ortho*-vanillin and hydrazine, which selectively and sensitively detects $Cu^{2+}$ both colorimetrically and fluorometrically among a series of different metal ions.

# Experimental

### General information

All the required materials used for synthesis were obtained from Sigma-Aldrich and directly used. Analytical-grade solvents were used for the overall experiments, and freshly prepared double-deionized water was used for dilution and preparing *tris* HCl buffer (10 μM, pH = 7.2) solution. The metal ion solutions were prepared from their nitrate salts. $^1$H NMR and $^{13}$C NMR spectra were recorded on a Bruker DRX spectrometer operating at 400 MHz in $CDCl_3$ solvent, and chemical shifts were recorded in ppm relative to TMS. Melting point was determined on an X-4 digital melting-point apparatus and was not corrected. Absorption spectra were recorded on a Shimadzu UV 1800 spectrophotometer using 10 mm path length quartz cuvettes with the wavelength in the range of 200–800 nm. Fluorescence spectra were recorded on a Hitachi spectrophotometer. Electrospray ionisation mass spectra (ESI-MS) were recorded on a Waters mass spectrometer using the mixed HPLC grade solvent methanol and triple distilled water. The pH adjustments were monitored using a digital pH meter (Merck) in buffer solution and adjusting with dilute hydrochloric acid and sodium hydroxide. Solutions of the receptor **$H_2L$** ($1 \times 10^{-5}$ M) and metal salts ($1 \times 10^{-4}$ M) were prepared in methanol–*tris*-HCl buffer (10 mM, pH 7.2) medium (1 : 1 v/v) and $H_2O$, respectively.

### X-Ray data collection and structure determination

Single-crystal X-ray data were collected using MoKα ($\lambda$ = 0.7107 Å) radiation on a Bruker APEX II diffractometer equipped with a CCD area detector. Data collection, data reduction, and structure solution/refinement were carried out using the software package of SMART APEX.[52] The structures were solved by direct methods (SHELXS-97) and standard Fourier techniques, and refined on $F^2$ using full-matrix least-squares procedures (SHELXL-97) using the SHELX-97 package[53] incorporated in WinGX.[54] In most cases, non-hydrogen atoms were treated anisotropically. Hydrogen atoms were fixed geometrically at their calculated positions following the riding atom model. The crystallographic data of **$H_2L$** and its Cu(II) complex **(1)** are listed in Table 1. Structural information for **$H_2L$** and **1** was deposited at the Cambridge Crystallographic Data Center (CCDC 2087278 and 2087279, respectively).

### Synthesis of $H_2L$

The ligand was synthesized by following a reported procedure.[55] *o*-Vanillin (0.304 g, 2 mmol) was dissolved in 10 mL dry methanol, and to this 0.05 g hydrazine hydrate (1 mmol) was added dropwise with constant stirring. Then, the reaction mixture was refluxed for 4 h under dry condition. After reflux, the reaction mixture was kept in air for evaporation; a light-yellow solid crystal separated out. Yield, 0.255 g, 85%. Anal. calc. For $C_{16}H_{16}N_2O_4$: C, 63.99; H, 5.37; N, 9.33%. Found: C, 63.86; H, 5.49; N, 9.26%. ESI–MS: *m*/*z* 301.1 (**$H_3L^+$**) (Fig. S1, ESI†).

Table 1 Crystallographic data and refinement parameters of the probe **$H_2L$** and its trinuclear Cu(II) complex (**1**)

| Identification code | **$H_2L$** | **1** |
|---|---|---|
| Empirical formula | $C_{16}H_{16}N_2O_4$ | $C_{32}H_{32}Cu_3N_6O_{16}$ |
| CCDC number | 2087278 | 2087279 |
| Formula weight | 300.31 | 947.25 |
| Temperature/K | 296.15 | 296.45 |
| Crystal system | Monoclinic | Triclinic |
| Space group | $P2_1$ | $P\bar{1}$ |
| *a*/Å | 5.701(3) | 8.157(7) |
| *b*/Å | 17.733(10) | 9.902(9) |
| *c*/Å | 6.535(4) | 11.983(9) |
| $\alpha$/° | 90 | 75.79(2) |
| $\beta$/° | 106.388(9) | 85.79(2) |
| $\gamma$/° | 90 | 87.08(3) |
| Volume/Å$^3$ | 633.8(6) | 935.2(14) |
| *Z* | 2 | 1 |
| $\rho_{calc}$ /g cm$^{-3}$ | 1.574 | 1.682 |
| $\mu$/mm$^{-1}$ | 0.115 | 1.771 |
| *F*(000) | 316.0 | 481.0 |
| Crystal size/mm$^3$ | 0.28 × 0.21 × 0.19 | 0.32 × 0.24 × 0.18 |
| Radiation | MoKα ($\lambda$ = 0.71073) | MoKα ($\lambda$ = 0.71073) |
| 2$\theta$ range for data collection/° | 4.594 to 53.832 | 4.81 to 50.75 |
| Index ranges | $-7 \le h \le 7$, $-22 \le k \le 22$, $-8 \le l \le 8$ | $-9 \le h \le 9$, $-11 \le k \le 10$, $-14 \le l \le 14$ |
| Reflections collected | 8607 | 6361 |
| Independent reflections | 2687 [$R_{int}$ = 0.0634, $R_{sigma}$ = 0.0851] | 3325 [$R_{int}$ = 0.0866, $R_{sigma}$ = 0.1465] |
| Data/restraints/parameters | 2687/13/203 | 3325/0/262 |
| Goodness-of-fit on $F^2$ | 1.240 | 1.024 |
| Final *R* indexes [$I >= 2\sigma$ (*I*)] | $R_1$ = 0.0537, w$R_2$ = 0.1114 | $R_1$ = 0.0748, w$R_2$ = 0.1706 |
| Final *R* indexes [all data] | $R_1$ = 0.1483, w$R_2$ = 0.1456 | $R_1$ = 0.1347, w$R_2$ = 0.2081 |
| Largest diff. peak/hole/e Å$^{-3}$ | 0.21/−0.25 | 0.71/−0.84 |

FTIR/$cm^{-1}$ (KBr): 3275 (vb, O–H), 1662 (vs, C═N), 1589 (m), 1446 (m), 1217 (s), 984 (m), 864 (m), 686 (s) (Fig. S2, ESI†).$^{1}$H NMR (400 MHz, $CDCl_3$, TMS): $\delta$ 11.55 (s, 2H, –OH), 8.71 (s, 2H, –C═NH), 7.20–6.91 (m, 6H, ArH), 3.95 (s,6H, $OCH_3$) (Fig. S3, ESI†).$^{13}$C NMR (100 MHz, $CDCl_3$, TMS): $\delta$ 164.79, 149.75, 148.39, 124.08, 119.42, 117.39, 115.22, 56.24 (Fig. S4, ESI†).

### Synthesis of $H_2L$–$Cu^{2+}$ complex $[Cu_3L_2(NO_3)_2(H_2O)_2]$) (1)

An aqueous–methanolic solution (10 mL, 1 : 1 v/v) of $Cu(NO_3)_2 \cdot 9H_2O$ (0.166 g, 0.5 mmol) was added dropwise to the hot stirring solution of **$H_2L$** (0.30 g, 1 mmol) in methanol–$H_2O$ (10 mL, 1 : 1 v/v). Immediate colour change was observed from colourless to reddish yellow. The solution was then stirred for 5 min at room temperature. The clear solution was kept for evaporation to obtain a red crude product. Yield, 0.510 g, 53.61%. The obtained product was recrystallised through diffusion from different phases *via* making a series of setups with different concentrations in DCM and diethyl ether; a red crystal suitable for single-crystal XRD analysis was obtained. Anal. calc. for $C_{32}H_{34}N_6O_{16}Cu_3$: C, 40.49; H, 3.61; N, 8.85%. Found: C, 40.65; H, 4.43; N, 8.97%. ESI–MS: *m*/*z* 722.5 (2**L** + $3Cu^{2+}$) (Fig. S5, ESI†). FTIR/$cm^{-1}$ (KBr): 3064 (wb), 1650 (vs), 2565 (s), 1275 (m), 1178 (s) (Fig. S6, ESI†).

### Computational details

The program package GAUSSIAN-09 Revision C.01 was employed for all calculations.[56] The gas phase geometries of the compound were fully optimized with symmetry restrictions in singlet ground state and the gradient-corrected DFT level coupled with B3LYP.[57] Basis set LanL2DZ was used for the whole molecules **$H_2L$** and $[Cu_3L_2(NO_3)_2(H_2O)_2]$ (**1**). The HOMOs and LUMOs of molecular ions were calculated with the same basis set and functional.

### Preparation of stock solution for photophysical measurements

Receptor **$H_2L$** solution was prepared initially at the concentration of $1 \times 10^{-3}$ M in 10 mL methanol–*tris* HCl buffer medium (10 mM, pH 7.2) solution (1 : 1 v/v), then diluted to the desired concentration. Stock solutions of guest ions were prepared separately from their nitrate salts (except for the sulphate salt of $Fe^{2+}$, ammonium heptamolybdate salt for $Mo^{6+}$ and the potassium salts for $Cr^{6+}$ and $Mn^{7+}$) at a concentration of $1 \times 10^{-3}$ M in 10 mL double-deionised water and further diluted to their desired concentrations. After mixing **$H_2L$** with each of the metal ions for a few seconds, absorption and fluorescence spectra were obtained at room temperature.

### Job's plot measurements

A methanol–*tris*-HCl buffer (1 : 1 v/v, 10 mM, pH 7.2) solution containing **$H_2L$** (10 μM) and an aqueous solution of $Cu(NO_3)_2$ were prepared separately. Then, the mole ratio of **$H_2L$** was changed from 0.1 to 0.9 in such a manner that the sum of the total volume of metal ions and **$H_2L$** remained constant (2 mL). All solutions were diluted to 3 mL. After shaking them for a minute, UV–vis spectra were obtained at room temperature.

## Results and discussion

### Structure establishment of ligand ($H_2L$)

The condensation reaction between *o*-vanillin and hydrazine in a 2 : 1 proportion produced Schiff base receptor **$H_2L$** as a yellow solid in good yield, and it was mainly characterised by elemental analysis, FTIR spectra, ESI-MS, $^{1}$H-NMR spectra and single-crystal XRD analysis. The compound showed excellent solubility in common solvents such as acetonitrile (ACN), dimethyl sulphoxide (DMSO), methanol (MeOH) and dichloromethane (DCM) but not in pure water (Scheme 1). In our present study, methanol is used to improve water solubility of the probe **$H_2L$**. To investigate the stability of ligand **$H_2L$** in 1 : 1 MeOH–$H_2O$ medium at room temperature, ESI-mass spectrum was recorded (Fig. S1, ESI†). Here, the presence of an intense molecular ion peak at *m*/*z* = 300.1 confirms the solution stability of **$H_2L$**. In the FTIR spectra of **$H_2L$**, the broad band appearing at 3480 $cm^{-1}$ is due to phenolic OH, and the sharp peak at 1620 $cm^{-1}$ is due to the C═N group. From the $^{1}$H-NMR spectra, characteristic singlet peaks were obtained at 11.62, 9.89 and 1.32 ppm respectively due to –OH, –C═N and –OMe groups, along with peaks between 7.62 to 7.36 ppm for aromatic protons. The compound **$H_2L$** displayed intense absorption bands at 313 nm and 225 nm, and a small hump at 390 nm, which imparts its very light-yellow color in 1 : 1 aqueous methanol. Here, the band at 313 nm and 225 nm originated because of the n–π* and π–π* electronic transitions. Also, in the fluorescence study of the receptor **$H_2L$** in this medium, a broad maximum was obtained around 360 nm when excited at 310 nm.

Slow evaporation of a moderately concentrated methanolic solution of the probe **$H_2L$** yielded a fine, needle-shaped crystalline form suitable for single-crystal XRD. The shortest imine-based salen derivative, the probe **$H_2L$** is a 3-methoxy 2-hydroxy aldazine in which the two units of salicylaldehyde derivative are linked directly through imine nitrogen atoms. There are rotational degrees of freedom about the central N–N bond. **$H_2L$** is crystallized in the monoclinic system with space group $P2_1$. The SCXRD studies revealed that **L** molecule is planar. The ORTEP view of **$H_2L$** with the atom numbering scheme is shown in Fig. 1. The bond length and bond angles are within the expected ranges. The methoxy groups, as well as the hydroxyl groups, are anti to each other. So, the molecule of **$H_2L$** adopts an anti-configuration in solid state. The N1–C1 (1.240 Å) and N1–N2 (1.346 Å) distances indicate agreement to double and single bonds, respectively. The torsion angle N1–C1–C2–C2 [−175.4°] specifies the molecule is essentially planar. Intramolecular O3–H···N1 and symmetry equivalent O4–H···N2 hydrogen bonds play an important role in stabilizing the geometry of **$H_2L$**, and in the crystal, the molecules are

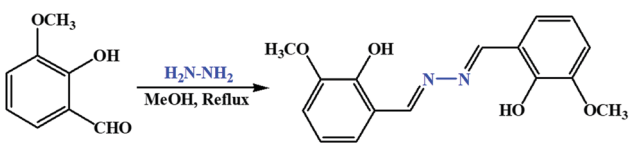


Scheme 1 Synthesis of the probe **$H_2L$**.

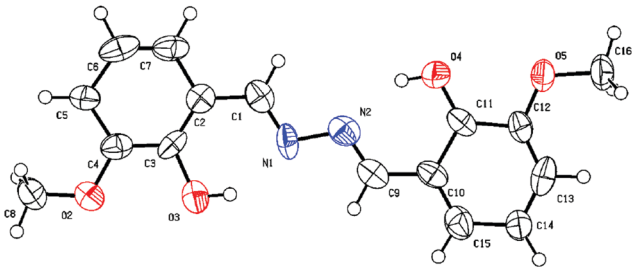


Fig. 1 ORTEP diagrams of $H_2L$ showing the atom-labeling scheme and 50% thermal ellipsoids.

interlinked and stabilized through C–H···π (C4–C6) interactions in addition to van der Waals forces (Fig. S7, ESI†).

### Single-crystal structure of the Cu(II) complex of $H_2L$ (1)

**1** crystallized in the triclinic system with space group $P_1$. The SCXRD studies revealed that **1** is trinuclear. The ORTEP view of **1** with the atom numbering scheme is shown in Fig. 2. In the crystal structure of the Cu(II) complex, two different coordination environments of the Cu(II) centres are observed with two di-deprotonated ligands of $H_2L$ ($C_{16}H_{16}N_2O_4$) and three copper(II) ions. Two peripheral Cu(II) ions are fifth coordinated distorted trigonal bipyramidal, while the inner Cu(II) centre is sixth coordinated octahedral geometry. The TBP geometries of the peripheral Cu(II) ions have also been confirmed by the calculations of Addison parameter value $\tau$ = 0.883 ($\tau = \beta - \alpha/60$).[58] Fifth coordination of each of the two peripheral Cu(II) ions is satisfied by one imine–N atom, two phenoxide O atoms, and one O-atom of one –$OCH_3$ group of two different molecules of the ligand $H_2L$ and the O atom of the coordinated $H_2O$ molecule, with the corresponding bond distances Cu(II)–N(imi) = 1.934 Å, Cu(II)–O(pheoxide 1) = 1.875 Å, Cu(II)–O(pheoxide 2) = 1.974 Å, Cu(II)–O($OCH_3$) = 2.083 Å and Cu(II)–O($OH_2$) = 2.122 Å. The two peripheral Cu(II) ions are above and below the plane of the inner Cu(II) centre. The di-deprotonations of the two ligands ($H_2L$) balance the charges of the peripheral Cu(II) centres. The sixth coordination of the two inner Cu(II) ions is satisfied by two imine –N atoms and two phenoxide O atoms of different ligand molecules and two Cu(II)–O($NO_3$) bonds, with the respective distances of 1.978 Å, 1.949 Å and 2.516 Å. All the bond distances are in good agreement with previously reported structures. Three copper(II) ions are not in a straight line in the complex, and the atomic distance of Cu···Cu is 3.344 Å. Both Cu–O–Cu bond angles are 116.96°, whereas the Cu–N–N–Cu torsional angles are 30.18°. The metal ions are surrounded by the organic ligand and do not interact with one another. There is perfect face-to-face π–π stacking with a distance 3.755 Å, and in the crystal structure of **1**, there are several OH···H hydrogen-bonding interactions between coordinated $H_2O$ molecules and $NO_3$ counter-ions (Fig. S8, ESI†).

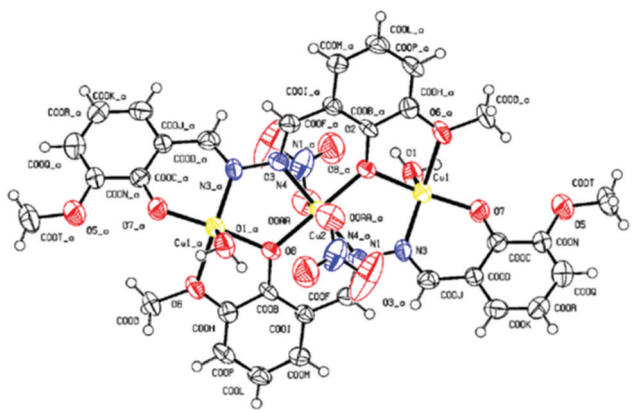

Fig. 2 ORTEP diagrams of **1** showing the atom-labeling scheme and 50% thermal ellipsoids.

### Absorption selectivity studies

Initially, the selectivity of chemosensor $H_2L$ towards various metal ions was observed by naked eyes, along with absorption studies at room temperature in methanol–*tris*-HCl buffer (1 : 1 v/v, 10 mM, pH 7.2) solution. On systematic addition of 5 equiv. of different metal ions (*e.g.*, $Fe^{3+}$, $Co^{2+}$, $Ni^{2+}$, $Cu^{2+}$, $Zn^{2+}$, $Cd^{2+}$, $Hg^{2+}$, $Pb^{2+}$, $Mo^{6+}$, $Cr^{3+}$, $Ag^{+}$, $Al^{3+}$, $Mn^{2+}$, $Fe^{2+}$, $Cr^{6+}$ and $Mn^{7+}$) to a fixed amount of $H_2L$, no colour change from colourless to yellow (Fig. 3) and no spectral change (Fig. 4) were observed in all cases except $Cu^{2+}$ and $Mo^{6+}$. An intense peak, developed at 274 nm, and increased absorbance intensity at 313 nm for $H_2L$ were observed in presence of 5 equiv. $Mo^{6+}$ ion; in the case of the addition of $Cu^{2+}$ ion, a new peak developed at 434 nm. In the competitive experiments, the metal ($Cu^{2+}$)-dependent absorption spectra of $H_2L$ was not disturbed in the presence of the remaining metal ions. The characteristic absorption band at 434 nm for $H_2L$–$Cu^{2+}$

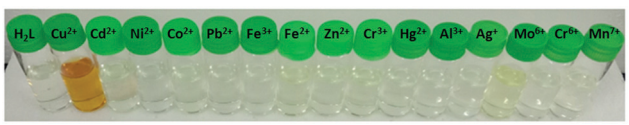


Fig. 3 Colour change in visible light of probe $H_2L$ on addition of different metal ions.

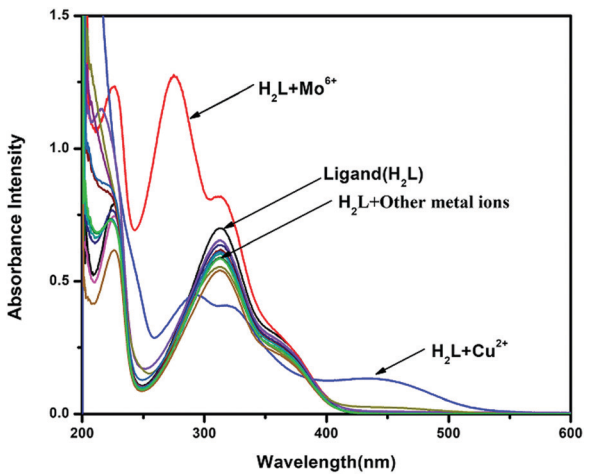


Fig. 4 Absorption spectra of $H_2L$ (10 μM) changes in the presence of 5 equiv. of different metal ions.

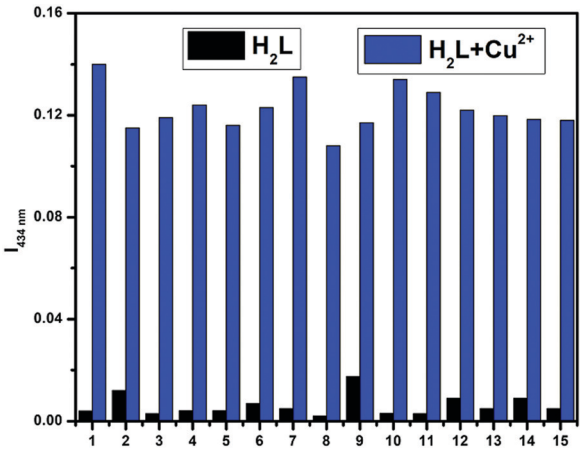


Fig. 5 Competitive experiment of $\mathbf{H_2L}$–$Cu^{2+}$ with other metal ions where 1 = $\mathbf{H_2L}$, 2 = $Mo^{6+}$, 3 = $Cd^{2+}$, 4 = $Pb^{2+}$, 5 = $Fe^{3+}$, 6 = $Fe^{2+}$, 7 = $Ni^{2+}$, 8 = $Al^{3+}$, 9 = $Zn^{2+}$, 10 = $Co^{2+}$, 11 = $Hg^{2+}$, 12 = $Cr^{3+}$, 13 = $Ag^{+}$, 14 = $Cr^{6+}$, 15 = $Mn^{7+}$.

remained almost consistent, with negligible loss of intensity, when 5-fold higher concentrations of interfering ions were added in the host–guest solution. Even the 10-fold higher concentration of $Mo^{6+}$ ion does not interfere with the absorption of $\mathbf{H_2L}$–$Cu^{2+}$ (Fig. 5).

### Absorption titration and LOD

In the absorption titration experiments, upon incremental addition of aqueous $Cu^{2+}$, the absorbance intensity at 313 was steadily decreased with the generation of a new peak at 434 nm, accompanied by 121 nm bathochromic shift. Thus, two clear isosbestic points at 355 nm and 390 nm developed, which indicate that $\mathbf{H_2L}$ and its $Cu^{2+}$ adduct are present in equilibrium (Fig. 6a). The limit of detection (LOD) for $Cu^{2+}$ was calculated from these titration curves by linear fitting of the intensity at 434 nm *vs.* $[Cu^{2+}]$. The obtained LOD value is $7.1 \times 10^{-8}$ M for $Cu^{2+}$, calculated using the formula 3(SD/*S*), where 'SD' is the measured standard deviation of the blank sample and '*S*' is the slope of the linear fitted calibration curve (Fig. 6b).

### Stoichiometry and association constant

Conventional Job's continuation method of variation indicates that two $\mathbf{H_2L}$ molecules can coordinate with three $Cu^{2+}$ ions (Fig. S9, ESI†), which was further established by ESI-MS analysis. The base peak was obtained at $m/z$ = 722.5, which corresponds to $[Cu_3L_2]^{2+}$ (Fig. S5, ESI†). To support the $Cu_3L_2$ complexation in solid phase, isolation in single-crystal form is also necessary, as it is more acceptable in current research. Thus, sincere efforts were made to isolate the **L**–$Cu^{2+}$ complex in the form of single crystal at the experimental condition. Mixing of each receptor–analyte in a 2 : 1 molar ratio, a block-shaped red crystal was separated out, which was suitable for single-crystal XRD (*vide supra*).

Considering the binding ratio, the association constant was calculated to be $7.7 \times 10^{7}$ $M^{-3/2}$ by the linear fitting of Benesi–Hildebrand (B–H) equation $1/(A - A_0)$ *vs.* $1/[Cu^{2+}]^{3/2}$ (Fig. S10, ESI†). However, the association constant values for other ions were too low to be calculated. This high binding value indicates the strong affinity of $Cu^{2+}$ ion towards the proposed chemosensor $\mathbf{H_2L}$.

### pH Experiment

The analyte binding affinity of receptor $\mathbf{H_2L}$ is also susceptible to the pH of the working media, as it contains –OH, >C═N, and –OMe groups, which are very sensitive to pH. Thus, receptor solutions with pH ranging from 2 to 13 were prepared in separate vials by adjusting with 0.1 M HCl and 0.1 M NaOH. Hence, each vial contains the same amount of $\mathbf{H_2L}$ at different pH values; absorption spectra were taken before and after analyte addition. From Fig. 7, the absorbance value of free ligand $\mathbf{H_2L}$ and its metal complex gradually increases from neutral to basic medium due to effective electrostatic interaction between the negatively charged $\mathbf{H_2L}$ and the positively charged metal ion. Therefore, all the sensing studies were performed at the physiological pH of 7.2, maintained by using *tris*-HCl buffer, where the acid–base sensitive groups cannot be disturbed.

### Reversibility studies

The reversible behaviour of the chemosensor $\mathbf{H_2L}$ was verified using $Na_2EDTA$. When the $\mathbf{H_2L}$ +$Cu^{2+}$ adduct was treated with

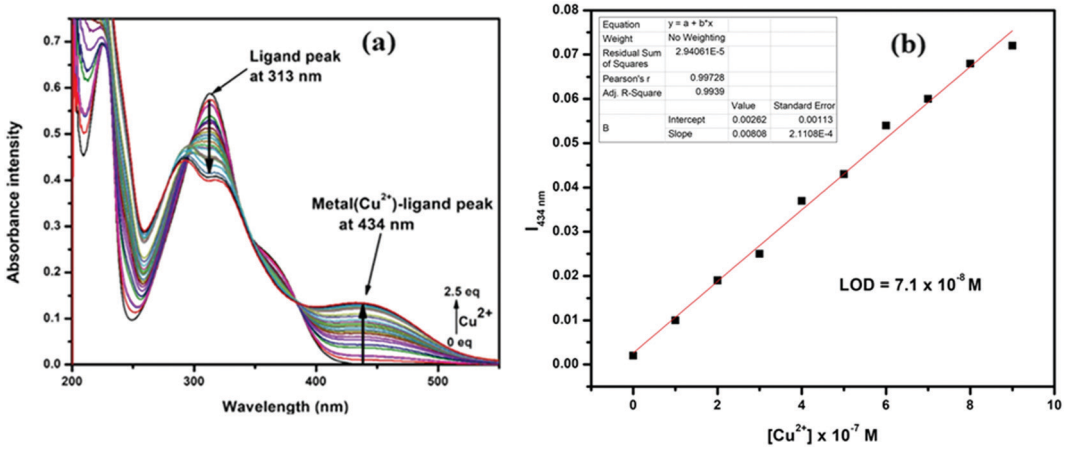


Fig. 6 (a) UV-vis titration of $\mathbf{H_2L}$ with $Cu^{2+}$, (b) detection limit.

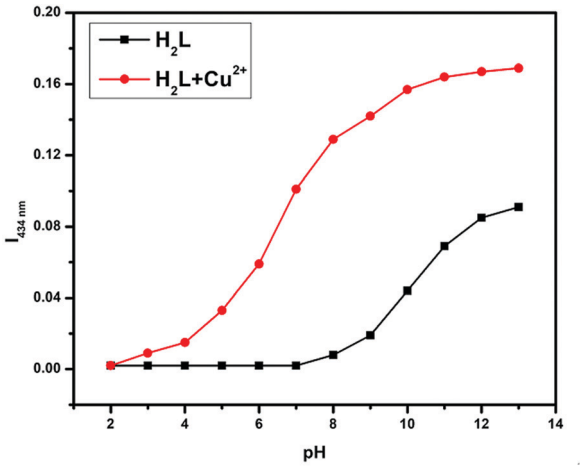


Fig. 7 pH effect of $H_2L$ and $H_2L$–$Cu^{2+}$ at 434 nm.

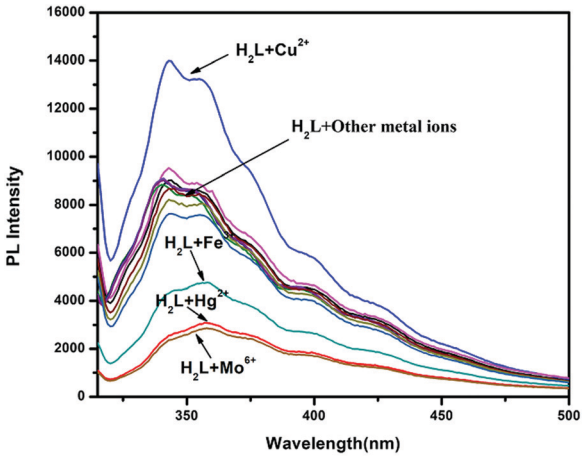


Fig. 9 Fluorescence spectra of $H_2L$ with different cations.

$Na_2EDTA$ (Fig. 8), the metal-induced absorption bands at 434 nm immediately vanished, with the simultaneous appearance of the original absorption band of free $H_2L$ at 313 nm, accompanied by visual color change from yellow to colourless. With excessive addition of $Cu^{2+}$ ion into the resultant solution, absorbance intensity was almost recovered. The absorption band switching between $H_2L$ and $H_2L$–$Cu^{2+}$ was regularly observed for more than 5 cycles with negligible loss of intensity. This observation clearly indicates that metal ions coordinate *via* chelation rather than any acid catalyst irreversible reaction.

### Fluorescence property

To check the emission selectivity of $H_2L$ towards metals, steady-state fluorescence experiments were separately performed with $Fe^{3+}$, $Co^{2+}$, $Ni^{2+}$, $Zn^{2+}$, $Cd^{2+}$, $Hg^{2+}$, $Pb^{2+}$, $Mo^{6+}$, $Cr^{3+}$, $Ag^{+}$, $Al^{3+}$, $Mn^{2+}$, $Fe^{2+}$, $Cr^{6+}$ and $Mn^{7+}$ in methanol–*tris*-HCl buffer (1 : 1 v/v, 10 mM, pH 7.2) solution. The receptor $H_2L$ displayed moderate fluorescence at 360 nm when excited at 310 nm (fluorescence quantum yield, $\Phi = 0.007$). This emission intensity was enhanced only in the presence of $Cu^{2+}$ ions (fluorescence quantum yield, $\Phi = 0.013$), whereas $Mo^{6+}$, $Hg^{2+}$ and $Fe^{3+}$ ions showed selective quenching behavior (Fig. 9). The other metal ions showed negligible change in the emission spectra of $H_2L$, even in the presence of more than 5-fold higher amounts than $Cu^{2+}$. In the titration experiments, with gradual addition of $Cu^{2+}$ ions to the receptor solution, the emission intensity continuously enhanced and became saturated when [$Cu^{2+}$] reached 1.5 equiv. Here, emission was enhanced due to restriction of both PET and C=N-isomerisation process after metal binding; thus, fluorescence was enhanced due to the chelation enhancement fluorescence (CHEF) process. The fluorometric detection limit was 0.038 μM (Fig. 10), which is slightly different from values obtained from UV-Vis spectra.

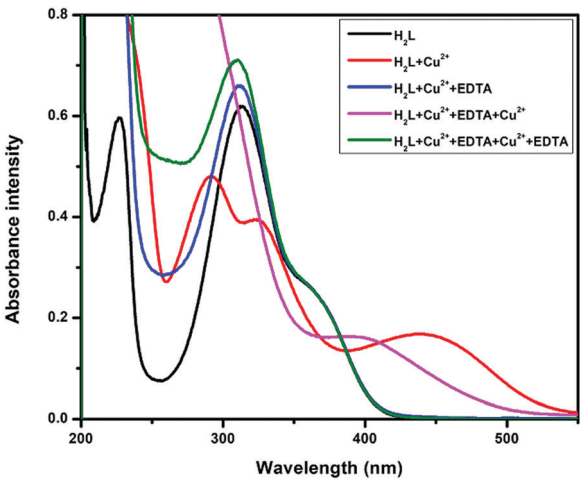


Fig. 8 Reversible investigation of $H_2L$ and $Cu^{2+}$ with EDTA.

### DFT studies on fluorescence properties

The probe $H_2L$ shows a straightforward approach for the selective detection of $Cu^{2+}$, with enhancement of fluorescence in conjunction with red shift (10 nm) because of chelation-enhanced fluorescence (CHEF) and internal charge transfer (ICT) processes after interaction with $Cu^{2+}$. The energy gap between the highest occupied molecular orbital (HOMO) and lowest unoccupied molecular orbital (LUMO) of $H_2L$ and its Cu(II) complex (**1**) are 5.55 eV and 2.11 eV, respectively. The complex **1**, compared to $H_2L$, established easy electronic transition and obtains the additional stability from **1** (Fig. 11). The contours of the electronic distribution in HOMO and LUMO states of these molecules suggest significant energy difference, 3.44 eV, between $H_2L$ and (**1**). Specifically, both the HOMO and LUMO states of the copper complex **1**, in comparison to $H_2L$, reveal that the electrons are more delocalized in the **1** molecule than the $H_2L$, in accordance with the barrier of photo-induced electron transfer process, which may result in the enhancement of fluorescence through CHEF.

### Application of chemosensor $H_2L$ in real samples

To explore the $Cu^{2+}$ sensing ability of the present chemosensor $H_2L$ in real water samples, we initially tested using laboratory tap water and distilled water samples. The ion concentration of

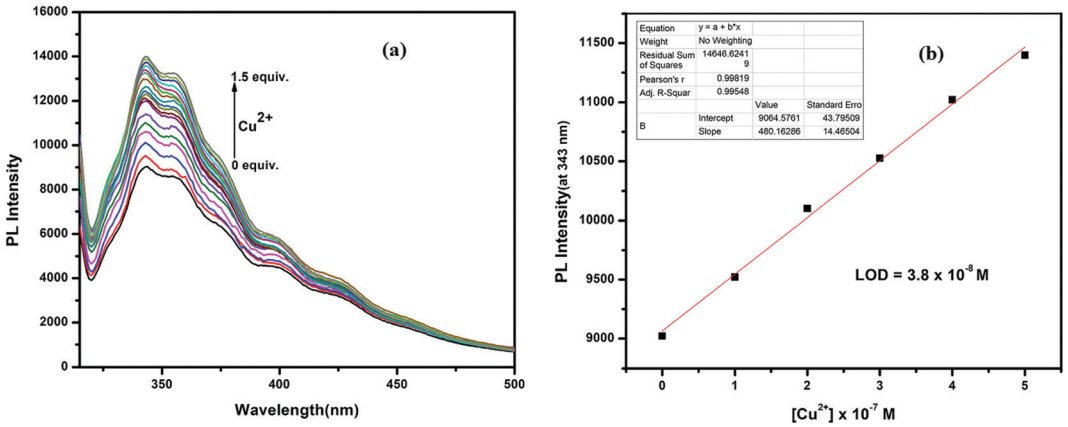


Fig. 10 (a) Fluorescence titration of $H_2L$ with $Cu^{2+}$ and (b) fluorescence detection limit.

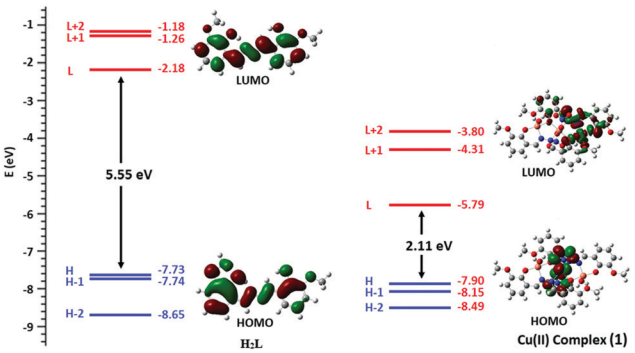


Fig. 11 Energy level diagram for the frontier MOs of $H_2L$ (left) and $Cu_3L_2$ complex (**1**) (right).

these samples could not be measured by this method as the laboratory tap water and distilled water samples didn't content $Cu^{2+}$. We then tested the probe $H_2L$ in waste water, and we obtained some results. To check its sensing in different samples, tap water samples artificially contaminated with $Cu^{2+}$ were prepared by adding known amounts of standard $Cu^{2+}$ solutions. The prepared samples were analyzed by the same UV-vis spectrometry method, and the recovery amounts were calculated using the calibration curve (intensity *vs.* conc.) with the help of Beer–Lambert law. As shown in Table 2, the $Cu^{2+}$ concentrations recovered for each sample are in close agreement with the spiked amounts, with good precision. Thus, the receptor $H_2L$ is suitable for detecting $Cu^{2+}$ ions quantitatively in real water samples, indicating that it could be applied in real environments.

## Comparison of $H_2L$ with other fluorescent and colorimetric chemosensors

The performance of the sensing action of the probe $H_2L$ towards $Cu^{2+}$ was compared with some other reported chemosensors, as listed in Table 3. Compared to the other systems, our system has several attractive analytical features, such as high sensitivity, wide linear range, high selectivity, lower detection limit, simple operation technology, good solubility,

Table 2 Analysis of $Cu^{2+}$ (μM) in water samples by the developed method (mean ± standard deviation, $n$ = 3)

| Sample | $Cu^{2+}$ added | $Cu^{2+}$ found | Recovery (%) | Relative error (%) |
|---|---|---|---|---|
| Waste water | 0 | 0.72 ± 0.89 | — | — |
| | 5 | 5.13 ± 0.97 | 102.6 | 2.6 |
| | 10 | 10.15 ± 1.54 | 101.5 | 1.5 |
| | 20 | 19.70 ± 0.87 | 98.5 | 1.5 |
| Tap water | 0 | ND | — | — |
| | 5 | 4.81 ± 1.3 | 96.2 | 3.8 |
| | 10 | 10.12 ± 0.93 | 101.2 | 1.2 |
| | 20 | 20.06 ± 1.2 | 100.3 | 0.6 |
| Distilled water | 0 | ND | — | — |
| | 5 | 5.02 ± 1.5 | 100.5 | 0.4 |
| | 10 | 9.87 ± 1.1 | 98.7 | 1.3 |
| | 20 | 19.96 ± 1.5 | 99.8 | 1.0 |

ND = not detected.

sensitive visualization and good practical applicability. Moreover, the synthesis of our proposed chemosensor $H_2L$ requires only two steps and less hazardous reagents, and no hazardous by-product is formed.

## Molecular logic gate application

The interesting optical behaviour of the probe $H_2L$ was demonstrated by establishing a molecular logic gate. Herein, the logic characteristics of probe $H_2L$ can also be viewed as a two-input-one-output "IMPLICATION" and "INHIBIT" logic gate in water media. Taking the idea from different absorption intensities in the UV-Vis spectra of developed probe $H_2L$ and its behavior with metal ions, logic operations with $Cu^{2+}$ as chemical input and absorption spectra as a channel output may be achieved. With addition of $Cu^{2+}$ to this ligand, a prominent absorbance band is observed at 434 nm, but upon addition of $Na_2EDTA$, the absorbance band at 434 nm vanishes. Hence, the INHIBIT logic gate is achieved. On the other hand, at 313 nm, decreased intensity was observed on addition of $Cu^{2+}$, which reappears on $Na_2EDTA$ addition. Thus, with two inputs, $H_2L$ has the ability to exhibit INHIBIT and IMPLICATION functions *via* absorbance

Table 3 Comparison of $H_2L$ with other reported chemosensors

| | | Limit of detection for $Cu^{2+}$(M) | | |
|---|---|---|---|---|
| Type of sensors | Ion sensing | Colorimetrically | Fluorometrically | References |
| Azine based | $Cu^{2+}$ | $7.1 \times 10^{-7}$ | $3.8 \times 10^{-7}$ (Turn-On) | Present work |
| | $Cu^{2+}$, $Fe^{3+}$ | $9.8 \times 10^{-7}$ | — | 59 |
| | $Cu^{2+}$ | $2.5 \times 10^{-6}$ | — | 60 |
| Dihydrazone based | $Cu^{2+}$ | $5.3 \times 10^{-7}$ | — | 48 |
| Chromone-based | $Cu^{2+}$ | $4.6 \times 10^{-7}$ | — | 61 |
| Quinoline-based | $Cu^{2+}$, $CN^-$ | $5.3 \times 10^{-7}$ | — | 62 |
| | $Cu^{2+}$, $Fe^{3+}$ | — | $1.35 \times 10^{-7}$ (Turn-Off) | 63 |
| Glycine based | $Cu^{2+}$ | $5.0 \times 10^{-7}$ | — | 64 |
| Triazole based | $Cu^{2+}$, $Pb^{2+}$ | $3.7 \times 10^{-6}$ | $1.24 \times 10^{-6}$ (Turn-On) | 46 |
| | $Cu^{2+}$ | — | $3.6 \times 10^{-9}$ (Turn-On) | 65 |
| Naphthalene-based | $Cu^{2+}$, cysteine | $1.07 \times 10^{-6}$ | — | 66 |

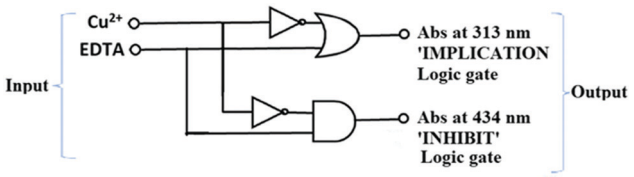


| Input | | Output | |
|---|---|---|---|
| $Cu^{2+}$ | $Na_2EDTA$ | Absorbance at 434 nm | Absorbance at 313 nm |
| 0 | 0 | 0 | 1 |
| 1 | 0 | 1 | 0 |
| 1 | 1 | 0 | 1 |
| 0 | 1 | 0 | 1 |

Fig. 12 IMPLICATION and INHIBIT logic gates and truth table.

output. The corresponding truth table, along with a sketch of the logic gate, is presented in Fig. 12.

## Conclusions

In summary, we have developed a novel azine-based fluorescent colorimetric sensor $H_2L$ for the selective and sensitive dual detection of $Cu^{2+}$. The chemosensor established the presence of the cation $Cu^{2+}$ by both UV-visible and fluorescence spectra, with an instant change of colour from colourless to intense yellow. LOD values of $H_2L$ towards $Cu^{2+}$ were calculated to be $7.1 \times 10^{-8}$ M (colorimetrically) and $3.8 \times 10^{-8}$ M (fluorometrically). The interaction between $H_2L$ and $Cu^{2+}$ were studied by Job's plot, ESI-MS, FT-IR spectroscopy and DFT calculations. Single-crystal structures both for the ligand $H_2L$ and its Cu(II) complex **1** were reported. Our developed probe $H_2L$ is much more efficient in comparison to other reported ligands. $H_2L$ can operate in a wide range of pH and be successfully applied for detection and quantification of $Cu^{2+}$ in various environmental samples, as well as for constructing INHIBIT and IMPLICATION type molecular logic gates.

## Conflicts of interest

Authors declare no conflicts of interest.

## Acknowledgements

G. K. P. would like to thank the Department of Science and Technology (SR/FST/CSI-264/2014 and EMR/2017/0001789), Government of India, New Delhi, for financial support. M. S. and A. K. M. gratefully acknowledge CSIR (New Delhi), Government of India, for financial support in the form of the research fellowships.

## References

1 R. Chandra, A. Ghorai and G. K. Patra, *Sens. Actuators, B*, 2018, **255**, 701.
2 P. Li, X. Duan, Z. Chen, Y. Liu, T. Xie, L. Fang, X. Li, M. Yin and B. Tang, *Chem. Commun.*, 2011, **47**, 7755.
3 N. J. Robinson and D. R. Winge, *Biochemistry*, 2010, **79**, 537.
4 X. Qi, E. J. Jun, L. Xu, S.-J. Kim, J. S. J. Hong, Y. J. Yoon and J. Yoon, *J. Org. Chem.*, 2006, **71**, 2881.
5 Z. Shi, X. Tang, X. Zhou, J. Cheng, Q. han, J. Zhou, B. Wang, Y. Yang, W. Liu and D. Bai, *Inorg. Chem.*, 2013, **52**, 12668.
6 P. G. Georgopoulos, A. Roy, M. J. Yonone-Lioy, R. E. Opiekun and P. J. Lioy, *J. Toxicol. Environ. Health, Part B*, 2001, **4**, 341.
7 H. Sigel and M. Dekker, Metal ions in biological systems in Properties of Copper, New York, USA, 1981.
8 J. A. Cowan, *Inorganic Biochemistry: An Introduction*, Wiley VCH, New York, NY, USA, 1997.
9 H. Kozlowski, M. Luczkowski, M. Remelli and D. Valensin, *Coord. Chem. Rev.*, 2012, **256**, 2129.
10 J. Xiong, X. Liu, Q. Y. Cheng, S. Xiao, L.-X. Xia, B.-F. Yuan and Y.-Q. Feng, *ACS Chem. Biol.*, 2017, **12**, 1636.
11 Z. Shi, X. Tang, X. Zhou, J. Cheng, Q. Han, J.-A. Zhou, B. Wang, Y. Yang, W. Liu and D. Bai, *Inorg. Chem.*, 2013, **52**, 12668.
12 X. Zhang, Y. Shiraishi and T. Hirai, *Org. Lett.*, 2007, **9**, 5039.
13 E. Gaggelli, H. Kozlowski, D. Valensin and G. Valensin, *Chem. Rev.*, 2006, **106**, 1995.
14 T. V. O'Halloran and V. C. Culotta, *J. Biol. Chem.*, 2000, **275**, 25057.

15 D. Strausak, J. F. B. Mercer, H. H. Dieter, W. Stremmel and G. Multhaup, *Brain Res. Bull.*, 2001, **55**, 15.
16 A. C. Rosenzweig and T. V. O'Halloran, *Curr. Opin. Chem. Biol.*, 2000, **4**, 140.
17 A. Singh, Q. Yao, L. Tong, W. C. Still and D. Sames, *Tetrahedron Lett.*, 2000, **41**, 9601.
18 G. E. Batley and T. M. Florence, *Mar. Chem.*, 1976, **4**, 347.
19 V. K. Gupta, A. K. Jain, G. Maheshwari, H. Lang and Z. Ishtaiwi, *Sens. Actuators, B*, 2006, **117**, 99.
20 X. Chen, M. J. Jou, H. Lee, S. Kou, J. Lim, S. W. Nam, S. Park, K. M. Kim and J. Yoon, *Sens. Actuators, B*, 2009, **137**, 597.
21 S. L. C. Ferreira, M. A. Bezerra, A. S. Santos, W. N. L. dos Santos, C. G. Novaes, O. M. C. de Oliveira, M. L. Oliveira and R. L. Garcia, *TrAC, Trends Anal. Chem.*, 2018, **100**, 1.
22 L. Ferńandez-López, B. Gómez-Nieto, M. J. Gismera, M. T. Sevilla and J. R. Procopio, *Spectrochim. Acta, Part B*, 2018, **147**, 21.
23 I. D. I. Calle, P. Pérez-Rodríguez, D. Soto-Gómez and J. E. López-Periago, *Microchem. J.*, 2017, **133**, 293.
24 A. P. S. Gonzales, M. A. Firmino, C. S. Nomura, F. R. P. Rocha, P. V. Oliveira and I. Gaubeur, *Anal. Chim. Acta*, 2009, **636**, 198.
25 T. Sun, Y. Li, Q. Niu, T. Li and Y. Liu, *Spectrochim. Acta, Part A*, 2018, **195**, 142.
26 L. Tian, J. Qi, K. Qian, O. Oderinde, Q. Liu, C. Yao, W. Song and Y. Wang, *J. Electroanal. Chem.*, 2018, **812**, 1.
27 A. Kawde, A. Ismail, A. R. Al-Betar and O. Muraza, *Microporous Mesoporous Mater.*, 2017, **243**, 1.
28 W. Zhu, X. Huang, Z. Guo, X. Wu, H. Yu and H. Tian, *Chem. Commun.*, 2012, **48**, 1784.
29 Y. H. Lee, N. Park, Y. B. Park, Y. J. Hwang and J. S. Kim, *Chem. Commun.*, 2014, **50**, 3197.
30 R. Sheng, P. Wang, Y. Gao, Y. Wu, W. Liu, J. Ma, H. Li and S. Wu, *Org. Lett.*, 2008, **10**, 5015.
31 I. Oehme and O. S. Wolfeis, *Microchim. Acta*, 1997, **126**, 177.
32 M. Benounis, N. Jafrezic-Renault, H. Halouani, R. Lamartine and I. Dumazet-Bonnamour, *Mater. Sci. Eng., C*, 2006, **26**, 364–368.
33 R. F. M. Elshaarawy, R. Ali, S. M. Saleh and C. Janiak, *J. Mol. Liq.*, 2017, **241**, 308.
34 S. M. Saleh, R. Ali and R. F. Elshaarawy, *RSC Adv.*, 2016, **6**, 68709.
35 G. Sivaraman, M. Iniya, T. Anand, N. G. Kotla, O. Sunnapu, S. Singaravadivel, A. Gulyani and D. Chellappa, *Coord. Chem. Rev.*, 2018, **357**, 50.
36 J. Ponniah S, S. K. Barik, A. Thakur, R. Ganesamoorthi and S. Ghosh, *Organometallics*, 2014, **33**, 3096.
37 G. Sivaraman, T. Anand and D. Chellappa, *RSC Adv.*, 2013, **3**, 17029.
38 S. J. Ranee, G. Sivaraman, A. M. Pushpalatha and S. Muthusubramanian, *Sens. Actuators, B*, 2018, **255**, 630.
39 V. K. G. Gangatharan, K. M. Palsamy, S. Gandhi, A. Jamespandi, A. Kandasamy, T. Arunachalam, A. Shenmuganarayanan, S. Balasubramaniyam and R. Jegathalaprathaban, *Sens. Actuators, B*, 2018, **255**, 3235.
40 L. N. Li, S. S. Shen, R. Y. Lin, Y. Bai and H. W. Liu, *Chem. Commun.*, 2017, **53**, 9986.
41 J. Wang, H. Chen, F. Ru, Z. Zhang, X. Mao, D. Shan, J. Chen and X. Lu, *Chem. – Eur. J.*, 2018, **24**, 3499.
42 Y. Ping, Z. Chen, Q. Ding, Q. Zheng, Y. Lin and Y. Peng, *Tetrahedron*, 2017, **73**, 594.
43 F.-U. Rahman, S.-B. Yu, S. K. Khalil, Y. P. Wu, S. Koppireddi, Z.-T. Li, H. Wang and D.-W. Zhang, *Sens. Actuators, B*, 2018, **263**, 594.
44 B. Kaur, N. Kaur and S. Kuma, *Coord. Chem. Rev.*, 2018, **358**, 13.
45 A. K. Manna, M. Sahu, K. Rout, U. K. Das and G. K. Patra, *Microchem. J.*, 2020, **157**, 104860.
46 K. Rout, A. K. Manna, M. Sahu, J. Mondal, S. K. Singh and G. K. Patra, *RSC Adv.*, 2019, **9**, 25919.
47 M. Sahu, A. K. Manna and G. K. Patra, *Inorg. Chim. Acta*, 2021, **517**, 120199.
48 M. Sahu, A. K. Manna, S. Chowdhury and G. K. Patra, *RSC Adv.*, 2020, **10**, 44860.
49 M. Sahu, A. K. Manna, K. Rout, J. Mondal and G. K. Patra, *Inorg. Chim. Acta*, 2020, **508**, 119633.
50 A. K. Manna, J. Mondal, K. Rout and G. K. Patra, *Sens. Actuators, B*, 2018, **275**, 350.
51 A. K. Manna, K. Rout, S. Chowdhury and G. K. Patra, *Photochem. Photobiol. Sci.*, 2019, **18**, 1512.
52 *SMART & SAINT Software Reference manuals, version 5.0*, Bruker AXS Inc., Madison,WI, 1998.
53 T. Gruene, H. W. Hahn, A. V. Luebben, F. Meilleur and G. M. Sheldrick, *J. Appl. Crystallogr.*, 2014, **47**, 462.
54 L. J. Farrugia, *WinGX: An Integrated System of Windows Programs for the Solution, Refinement and Analysis for Single Crystal X-ray Diffraction Data, version 1.80.01*, Department of Chemistry: University of Glasgow, 2003.
55 D. R. Gayakwad, S. R. Sarda, S. U. Tekale, R. B. Nawale, D. Rajani, J. B. Bharad and R. P. Pawar, *Int. J. Med. Med. Sci.*, 2020, **11**, 14.
56 M. J. Frisch, G. W. Trucks, H. B. Schlegel, G. E. Scuseria, M. A. Robb, J. R. Cheeseman, G. Scalmani, V. Barone, B. Mennucci, G. A. Petersson, H. Nakatsuji, M. Caricato, X. Li, H. P. Hratchian, A. F. Izmaylov, J. Bloino, G. Zheng, J. L. Sonnenberg, M. Hada, M. Ehara, K. Toyota, R. Fukuda, J. Hasegawa, M. Ishida, T. Nakajima, Y. Honda, O. Kitao, H. Nakai, T. Vreven, J. A. Montgomery, Jr., J. E. Peralta, F. Ogliaro, M. Bearpark, J. J. Heyd, E. Brothers, K. N. Kudin, V. N. Staroverov, R. Kobayashi, J. Normand, K. Raghavachari, A. Rendell, J. C. Burant, S. S. Iyengar, J. Tomasi, M. Cossi, N. Rega, J. M. Millam, M. Klene, J. E. Knox, J. B. Cross, V. Bakken, C. Adamo, J. Jaramillo, R. Gomperts, R. E. Stratmann, O. Yazyev, A. J. Austin, R. Cammi, C. Pomelli, J. W. Ochterski, R. L. Martin, K. Morokuma, V. G. Zakrzewski, G. A. Voth, P. Salvador, J. J. Dannenberg, S. Dapprich, A. D. Daniels, Ö. Farkas, J. B. Foresman, J. V. Ortiz, J. Cioslowski and D. J. Fox, *Gaussian 09, Revision C.01*, Gaussian Inc., Wallingford, CT, 2009.
57 A. D. Becke, *J. Chem. Phys.*, 1993, **98**, 5648.
58 A. W. Addison, T. N. Rao, J. Reedijk, J. van Rijn and G. C. Verschoor, *J. Chem. Soc., Dalton Trans.*, 1984, 1349.

59 N. Narayanaswamy and T. Govindaraju, *Sens. Actuators, B*, 2012, **161**, 304.
60 G. K. Patra, R. Chandra, A. Ghorai and K. K. Shrivas, *Inorg. Chim. Acta*, 2017, **462**, 315.
61 A. Mohammadi, B. Khalili and A. S. Haghayegh, *Spectrochim. Acta, Part A*, 2019, **222**, 117193.
62 C. Wu, J. Wang, J. Shen, C. Zhang, Z. Wu and H. Zhou, *Tetrahedron*, 2017, **73**, 5715.
63 B. Zhang, H. Liu, F. Wu, G. Hao, Y. Chen, C. Tan, Y. Tan and Y. Jiang, *Sens. Actuators, B*, 2017, **243**, 765.
64 N. H. Ly, C. Seo and S.-W. Joo, *Sensors*, 2016, **16** 1785.
65 S. Qiu, Y. Wei, T. Tu, J. Xiang, D. Zhang, Q. Chen, L. Luo and Z. Lin, *Food Chem.*, 2020, **317**, 126434.
66 S. A. Lee, J. J. Lee, J. W. Shin, K. S. Min and C. Kim, *Dyes Pigm.*, 2015, **116**, 131.